INORGANIC CHEMISTRY FRONTIERS

RESEARCH ARTICLE

View Article Online
View Journal | View Issue

Cite this: *Inorg. Chem. Front.*, 2024, **11**, 5636

Superhydrophobic fluorinated metal–organic framework (MOF) devices for high-efficiency oil–water separation†

Jiaqi Ma,‡[a] Mingshi Zhang,‡[a,b] Rui Feng,[c] Lu Dong,[a] Wei Sun[d] and Yanyuan Jia*[a,e]

Oil spills have been a persistent environmental challenge globally, resulting in severe long-term impacts. Thus, developing materials for efficient oil–water separation is crucial. Metal–organic frameworks (MOFs), as a rapidly emerging class of porous materials, have gained tremendous attention due to their ultra-high surface area. In this study, four fluorinated MOFs with UiO-66 topology were synthesized and characterized. Their hydrophobicity was tailored by varying the types and quantities of the fluorine-containing functional groups (–F or $-CF_3$) on the ligands. Among them, $2CF_3$-UiO-66 showed the highest hydrophobicity, with a water contact angle (WCA) of 145.9°, making it promising for adsorbing organic pollutants and as a hydrophobic coating material. $2CF_3$-UiO-66 powder efficiently reduced the concentration of 3,5-dichlorophenol (a model halogenated water pollutant) from 300 ppm to 23.4 ppm within 2 hours. Furthermore, $2CF_3$-UiO-66 was *in situ* coated on cotton (CT) and sponge (SP) to form composite materials, $2CF_3$-UiO-66@CT and $2CF_3$-UiO-66@SP. $2CF_3$-UiO-66@CT is superhydrophobic (WCA = 164.7°), flexible, and fire retardant. It efficiently separated water and nine organic solvents *via* filtration, meeting commercial standards of <0.01% water content in the filtered organic solvents. $2CF_3$-UiO-66@CT remains structurally intact after 20 filtration recycles, suggesting its durability. These advantages make the $2CF_3$-UiO-66@CT an ideal candidate for oil–water separation *via* filtration. Alternatively, $2CF_3$-UiO-66@SP, with a porous sponge backbone, is suitable for oil–water separation by adsorbing the organic phase efficiently (60–140 g g^{-1} adsorption capacity on nine organic solvents), and the adsorbed oil can be easily pumped out. Overall, we believe the fluorinated MOFs reported in this work have great potential for adsorption and superhydrophobic coating applications.

Received 26th June 2024,
Accepted 12th July 2024

DOI: 10.1039/d4qi01613k

rsc.li/frontiers-inorganic

1. Introduction

Oil leaks and spills frequently occur in accidents or during the extraction and transportation of petroleum products. Over 700 million liters of oil-containing wastewater enter the ocean globally each year.[1] Crude oil and petroleum products are immiscible with water and undergo diffusion, evaporation, emulsification, and dissolution in the ocean, ultimately leading to global migration and pollution.[2,3] Oil spills are catastrophic to ecosystems[3–5] and lead to waste of valuable petroleum resources. Furthermore, the costs of cleaning up oil spills worldwide annually range from ~108 million to over 65 billion USD.[6] Mechanical extraction and *in situ* burning are conventional methods for oil spill cleanup.[7,8] However, mechanical extraction exhibits disadvantages such as low efficiency and high energy consumption.[9] The oil combustion approach generates severe air pollution.[9,10] Therefore, developing efficient and eco-friendly materials for oil–water separation is highly desirable.

The utilization of hydrophobic porous materials represents an emerging approach to oil–water separation.[11] This method offers advantages such as high efficiency, cost-effectiveness, and environmental friendliness.[12] However, conventional porous materials, such as activated carbon and zeolite, have limited surface area and hydrophobicity, leading to low oil recovery rates and adsorption capacities.[13,14] Therefore, developing superhydrophobic porous materials is promising in addressing the oil–water separation problem. Metal–organic

[a]*College of Chemistry and Chemical Engineering, Inner Mongolia University, Hohhot 010021, P. R. China*
[b]*Department of Chemistry and Biochemistry, University of California, San Diego, La Jolla, California 92093, USA*
[c]*School of Materials Science and Engineering, Smart Sensing Interdisciplinary Science Center, Nankai University & TKL of Metal and Molecule Based Material Chemistry, Tianjin 300350, P. R. China*
[d]*Department of Chemistry, University of Michigan, Ann Arbor, MI 48109, USA*
[e]*Key Laboratory of Advanced Energy Materials Chemistry (Ministry of Education), Nankai University, Tianjin 300071, P. R. China*

†Electronic supplementary information (ESI) available. See DOI: https://doi.org/10.1039/d4qi01613k

‡These authors contributed equally to this work.

frameworks (MOFs) are crystalline porous materials with ultra-high surface areas, tunable pore sizes, and modifiable functional groups.[15] These properties allow MOFs to have wide applications in gas adsorption,[16–18] separation,[19,20] catalysis,[21–24] sensing,[25,26] and energy storage.[27,28] Moreover, the tunable porous nature of MOFs makes them promising candidates as adsorbents for dyes,[29,30] toxic ions,[31] and pesticide.[32,33] However, to meet the requirement of oil–water separation, the wettability of MOFs must be controlled. Ideally, MOFs with superhydrophobic surfaces are desired. MOFs are composed of metal nodes and ligands containing coordinating functional groups such as carboxyl groups in the structure. Current strategies to prepare hydrophobic MOF materials majorly include (1) using hydrophobic linkers, (2) post-synthetic modification, (3) creating surface roughness, and (4) forming composites of MOF with hydrophobic materials.[34] Using hydrophobic linkers has advantages over the other strategies because it alternates the MOF structure at the molecular level. In addition, direct synthesis of the MOF can be achieved once the ligands are ready. Hydrophobic moieties such as alkyl[35,36] or fluorine-containing functional groups[37,38] have been installed on the ligands in MOFs. Although it is known that incorporating fluorine-containing functional groups can increase the material hydrophobicity,[34] the effects of different fluorinated functional groups and their quantities on the hydrophobicity of MOFs have rarely been investigated and compared. However, understanding and establishing a relationship between the types and numbers of fluorine-containing groups and the material wettability are key to the design of superhydrophobic MOFs. Moreover, fluorinated materials are potentially flame-retardant,[39–41] which brings extra benefits for safe storage, transportation, and practical applications.[42] Another limitation of MOFs in practical applications is that they are usually synthesized as powders.[43] Recycling the MOF powder after use is challenging.[44–49]

In this work, we used the bottom-up method to synthesize four fluorinated UiO-66 (UiO stands for University of Oslo) MOF analogs, including 1F-UiO-66, 2F-UiO-66, 1CF_3-UiO-66, and 2CF_3-UiO-66. The introduction of fluorine-containing functional groups enhances the hydrophobicity of MOFs. We also investigated the factors influencing hydrophobicity in this system. We found that the –CF_3 group contributes significantly more to hydrophobicity than –F, and more fluorine-containing functional groups lead to higher hydrophobicity. Among them, 2CF_3-UiO-66 exhibits the highest hydrophobicity, with a water contact angle (WCA) as high as 145.9°, which can remove 3,5-dichlorophenol (a model halogenated pollutant) from water with a high efficiency of 92.2%. Thus, 2CF_3-UiO-66 was used for further evaluation. To make the 2CF_3-UiO-66 recyclable for oil–water separation, we prepared composites of 2CF_3-UiO-66 particles with cotton (2CF_3-UiO-66@CT) and sponge (2CF_3-UiO-66@SP). The resulting composite material 2CF_3-UiO-66@CT demonstrated superhydrophobicity (WCA > 150°) with a WCA of 164.7°, achieving oil–water separation efficiencies of up to 99.66% for nine organic solvents through filtration. Using gasoline and carbon tetrachloride as model solvents, the water residues in the collected filtrates are as low as 0.009% and 0.008%, respectively, meeting the commercial standard (Table 2, S8†). In addition, 2CF_3-UiO-66@CT is flame retardant compared to non-modified cotton. Due to the flexibility of cotton, 2CF_3-UiO-66@CT is suitable for oil–water separation *via* filtration. Alternatively, 2CF_3-UiO-66 showed a synergetic effect with the porous sponge backbone, 2CF_3-UiO-66@SP is good at oil–water separation *via* adsorption. For example, the carbon tetrachloride adsorption capacity of 2CF_3-UiO-66@SP reached 141.52 g g^{-1}. With the assistance of a pump, 2CF_3-UiO-66@SP continuously collects oil above water. In addition, the synthesized composite materials exhibit strong solvent stability, mechanical stability, and reusability.

2. Experimental section

2.1. Materials and characterization

All the reagent-grade starting materials and solvents were used without further purification as received from commercial suppliers. PANalytical Empyrean diffractometer X-ray diffractometer working at 40 kV, 40 mA was employed for the collection of ambient temperature. STA 449 F1 Jupiter was used to conduct thermogravimetric analyses in the temperature range of 25–700 °C under an argon atmosphere with a heating rate of 5 °C min^{-1}. A Bruker Avance NEO spectrometer was used to record ^{1}H-NMR at 600 or 500 MHz, and ^{19}F-NMR at 565 or 470 MHz. Scanning electron microscopy images were collected by a HITACHIS-4800 scanning electron microscope, and the electronic acceleration voltage was 10 kV. UV-vis was tested in the range of 600–200 cm^{-1} on a Hitachi in Japan. BOEN-85697E FT-IR spectrometer was used to record Fourier transform infrared spectra in the range of 4000–500 cm^{-1}. X-ray photoelectron spectroscopy was tested by Thermo SCIENTIFIC ESCALAB 250Xi. Adsorption test of water vapor and toluene vapor using static volumetric steam adsorption meter ZQ100C. Contact angle experiments were performed using the JC2000D1 instrument of Shanghai Zhongchen Digital Technology Equipment Company Limited. Each test droplet drop was 5 μL. The water content test was performed on the Shanghai-Hezhou-AKF-1 plus instrument. The limiting oxygen index was measured by using the JF-3 limiting oxygen index meter of Nanjing Jiangning Analytical Instrument Company.

2.2. Synthesis of fluorinated UiO-66

2.2.1. Synthesis of 1F-UiO-66. $ZrCl_4$ (0.0233 g, 0.1 mmol), 2-fluoroterephthalic acid (0.0184 g, 0.1 mmol), and benzoic acid (0.0122 g, 0.1 mmol) were fully dissolved in DMF (4 mL) in a kettle with polytetrafluoroethylene lining. The container was sealed and heated to 100 °C for 24 h in an oven. Then, the temperature was gradually lowered to 25 °C over 6 hours. The white precipitate was collected by filtration and dried under the vacuum. The fluorinated UiO-66, 1F-UiO-66, is obtained with an 18% yield.

For a detailed synthesis and characterization of 2F-UiO-66, 1CF_3-UiO-66, and 2CF_3-UiO-66, see ESI.†

2.3. Fabrication of 2CF_3-UiO-66 devices

2.3.1. Pretreatment of cotton and sponge. Cotton is cut to 1.5 × 1.5 × 0.5 cm size and washed thoroughly with ethanol (5 mL). Then, the cotton was dried in an oven at 75 °C for 6 h (Fig. S36†). The sponge is cut to 1.0 × 1.0 × 2.0 cm, and the remaining steps are the same as cotton (Fig. S37†).

2.3.2. Synthesis of 2CF_3-UiO-66@CT/SP. $ZrCl_4$ (0.0233 g, 0.1 mmol), 2,5-bis(trifluoromethyl)terephthalic acid (0.0302 g, 0.1 mmol), and benzoic acid (0.0122 g, 0.1 mmol) were completely dissolved in DMF (6 mL/8 mL) in a reaction kettle lined with polytetrafluoroethylene containing. The pretreated cotton/sponge was immersed in the solution. The reaction kettle was sealed and heated to 100 °C for 24 hours in an oven. Then, the reaction was programmablely cooled down to 25 °C within 6 hours. Then, the cotton/sponge composite materials were washed with ethanol to remove excess MOFs on the surface and dried under vacuum (Fig. S36 and S37†).

The loading capacity percentage of 2CF_3-UiO-66 on cotton/sponge was calculated according to the following equation:

$$\text{Loading capacity percentage} = (M_2 - M_1)/M_1 \times 100\% \quad (1)$$

M_1 is the dried weight of cotton/sponge, and M_2 is the dried weight of the 2CF_3-UiO-66@CT/SP composites. The loading capacity of 2CF_3-UiO-66@CT/SP is calculated as 27%/24%.

2.4. Oil adsorption test of 2CF_3-UiO-66@CT/SP

Place the 2CF_3-UiO-66@CT/SP composite materials on top of the clean 5 mL syringe and compress it firmly to fully obstruct the syringe needle. As various oil compounds are introduced into the syringe, the composite material's lipophilicity will adsorb the oil. Once saturated, any surplus oil will discharge from the syringe, facilitating the determination of the composite material's adsorption capacity. The calculation formula is as follows:

$$\text{Adsorption capacity} = (M_2/M_1) \times 100\% \quad (2)$$

M_1 and M_2 are the weights of 2CF_3-UiO-66@CT/SP composites before and after oil adsorption, respectively.

2.5. Oil–water separation device by gravity method

The 2CF_3-UiO-66@CT/SP composite material is placed on the top of the clean 5 mL syringe and compacted to ensure that the needle part of the syringe is completely blocked by the composite material so that a simple oil–water separation device is prepared and fixed on the iron platform. Mix the oil and water phases 4 mL and 3 mL, respectively, and slowly pour the mixed solution into the oil–water separation device. The oil phase flows into the beaker through the composite material, and the water phase is isolated in the device. The separation efficiency is calculated according to water, and the formula is as follows:

$$\text{Separation efficiency} = (M_2/M_1) \times 100\% \quad (3)$$

M_1 and M_2 is the weight of the aqueous solution before and after oil–water separation, respectively.

3. Results and discussion

We first designed and synthesized a series of fluorinated terephthalic acids (structures shown in Fig. 1b–e. See ESI† for their synthesis and characterization, Schemes S1–S4†) as ligands to construct UiO-66 MOFs. These fluorinated ligands include 2-fluoroterephthalic acid (1F-BDC), 2,6-difluoroterephthalic acid (2F-BDC), 2-trifluoromethylterephthalic acid (1CF_3-BDC), and 2,5-bis(trifluoromethyl)terephthalic acid (2CF_3-BDC). The corresponding UiO-66 MOFs were obtained using a solvothermal method by mixing the corresponding ligands and $ZrCl_4$ in DMF at 100 °C for 24 h (Fig. 1b–e, with an emphasis on the representative fluorinated moiety in the MOF structure). The synthesized MOFs were named after the ligands 1F-UiO-66, 2F-UiO-66, 1CF_3-UiO-66, and 2CF_3-UiO-66, respectively. The morphology and particle size of the four prepared MOFs were characterized by scanning electron microscopy (SEM). The nanoparticles have a similar size of 200 nm and form clusters (Fig. S14†). Powder X-ray diffraction (PXRD) patterns indicate the four MOFs are crystalline and structurally similar to UiO-66 (Fig. 1k).[50] Fourier transform infrared (FT-IR) spectra suggested the presence of characteristic C–F bond with peaks at 1070–1015 cm^{-1} for the fluorinated MOFs (Fig. S17†). X-ray photoelectron spectroscopy (XPS) results show the characteristic peak of F1s at 687.0 eV nearby (Fig. S18–S21†). These results demonstrate that the fluorinated ligands coordinated with Zr nodes, forming the UiO-66 topology.

After the structural characterization of the fluorinated UiO-66 MOFs, we next evaluated their hydrophobicity. We initially observed that all of the four prepared fluorinated UiO-66 MOF powders floated on the surface of the water (Fig. S22†). In contrast, the non-fluorinated UiO-66 quickly settled at the bottom, indicating that it is less hydrophobic than its fluorinated analogs. To systematically study the influence of the types and quantities of fluorinated functional groups on the hydrophobicity of the fluorinated UiO-66 MOFs, we conducted WCA measurements on the fluorinated MOF powders. The results showed that water droplets wet UiO-66 (Fig. 1f), 1F-UiO-66 (Fig. 1g), and 2F-UiO-66 (Fig. 1h). In contrast, the WCA of 1CF_3-UiO-66 and 2CF_3-UiO-66 reached 139.5° and 145.9°, respectively (Fig. 1i and j). Compared to –F, the –CF_3 functional group imparts greater hydrophobicity to the MOFs. In addition, as the number of fluorinated functional groups on the ligands increased, and fluorinated MOFs became more hydrophobic. In comparison, organic solvents such as dichloromethane, chloroform, carbon tetrachloride, toluene, petroleum ether, *n*-hexane, hexadecane, kerosene, and gasoline wet 1CF_3-UiO-66 and 2CF_3-UiO-66 effectively (Fig. S25†). Inspired by the wettability performance of 1CF_3-UiO-66 and 2CF_3-UiO-66 with water and organic solvents, we hypothesized that they are promising candidates for removing

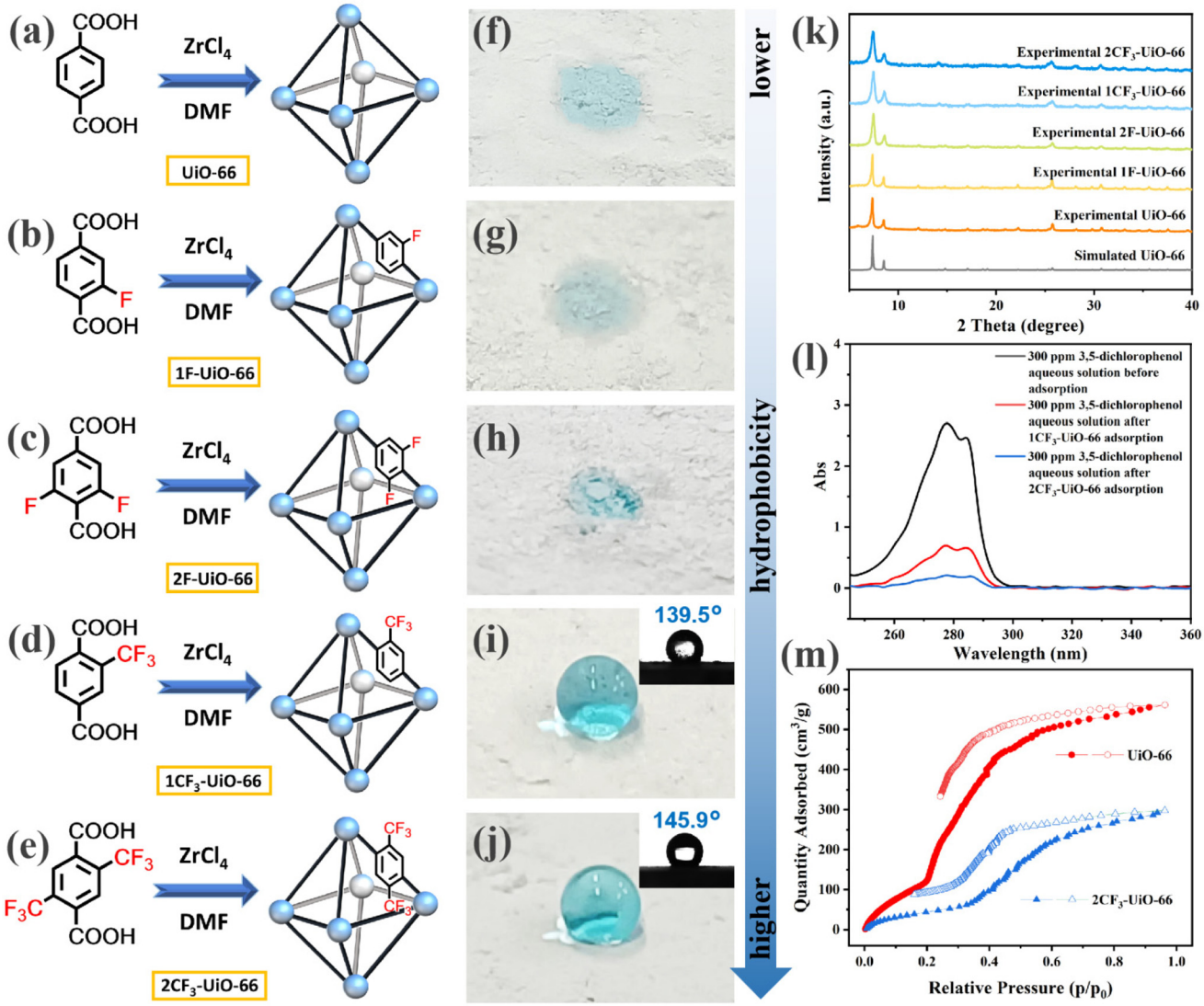

Fig. 1 (a–e) Schematic representation of the synthesis of UiO-66, 1F-UiO-66, 2F-UiO-66, 1CF_3-UiO-66, and 2CF_3-UiO-66. (f–j) Contact angle measurements *via* images of a water droplet on the surface of UiO-66, 1F-UiO-66, 2F-UiO-66, 1CF_3-UiO-66, and 2CF_3-UiO-66. (k) PXRD profiles of experimental data of UiO-66, 1F-UiO-66, 2F-UiO-66, 1CF_3-UiO-66, and 2CF_3-UiO-66 and the simulated data of UiO-66. (l) UV-vis adsorption spectra of 3,5-dichlorophenol aqueous solution (300 ppm) before and after treatment with 1CF_3-UiO-66 or 2CF_3-UiO-66. (m) Water adsorption isotherms for UiO-66 and 2CF_3-UiO-66.

lipophilic organic pollutants from water. Thus, the adsorption capacity of 1CF_3-UiO-66 and 2CF_3-UiO-66 was compared. A model halogenated organic pollutant, 3,5-dichlorophenol,[51] was dissolved in deionized water as a 300 ppm solution. 10 mg of 1CF_3-UiO-66 or 2CF_3-UiO-66 was mixed with 15 mL of the 3,5-dichlorophenol solution and subjected to ultrasonication for 2 h. The adsorption efficiency was measured using ultraviolet-visible (UV-vis) spectroscopy, with 1CF_3-UiO-66 and 2CF_3-UiO-66 achieving 74.1% and 92.2% removal efficiency for 3,5-dichlorophenol, respectively. Consequently, the residual 3,5-dichlorophenol concentration decreased to 77.7 and 23.4 ppm after treatment with 1CF_3-UiO-66 or 2CF_3-UiO-66 (Fig. 1l). This demonstrates that 2CF_3-UiO-66 has better adsorption efficiency than 1CF_3-UiO-66 toward organic pollutants.

We also characterized the water vapor adsorption and toluene vapor adsorption of UiO-66 and 2CF_3-UiO-66 (Fig. S28†). The results show that the adsorption amounts of water vapor (Fig. 1m) and toluene vapor (Fig. S29d†) by 2CF_3-UiO-66 are significantly lower than those by UiO-66 due to the occupation of void space by –CF_3 groups. Generally, if the interaction between gas molecules and MOFs is strong, the gas will be more easily captured at low concentrations. In other words, in the adsorption curve, a gas with strong interaction will exhibit a steep increase at a lower relative pressure (p/p_0). Both UiO-66 and 2CF_3-UiO-66 can cause toluene to fill or

condense in the pores at relatively low vapor pressures (p/p_0 < 0.1).[52,53] However, at ultra-low saturated vapor pressures, $2CF_3$-UiO-66 shows a higher adsorption capacity for toluene than UiO-66. Correspondingly, in the adsorption of water vapor, UiO-66 begins to fill rapidly at p/p_0 = 0.2, while the adsorption curve of $2CF_3$-UiO-66 does not become steep until p/p_0 = 0.35. These results indicate that both UiO-66 and $2CF_3$-UiO-66 are hydrophobic materials, but the hydrophobicity/lipophilicity of $2CF_3$-UiO-66 is significantly stronger than that of UiO-66.

From UiO-66 to $2CF_3$-UiO-66, the enhancement of hydrophobicity is attributed to the lower surface energy of fluorine-containing compounds. Previous studies have reported that the surface energy of compounds containing $-CF_3$ is lower than that of compounds containing –F.[34] We further calculated the free solvent energy of the ligand molecules terephthalic acid (BDC), 1F-BDC, 2F-BDC, $1CF_3$-BDC, $2CF_3$-BDC using water and the organic solvent octanol through computer simulation[54,55] (for the specific calculation methods, please refer to the ESI†). Based on the results, we further calculated the octanol–water partition coefficient. As shown in Table 1, the log ($P_{octanol}/P_{water}$) of BDC, 1F-BDC, 2F-BDC, $1CF_3$-BDC, and $2CF_3$-BDC increased, indicating that the hydrophobicity increased. Therefore, the most hydrophobic $2CF_3$-UiO-66 is more conducive to oil–water separation, which is consistent with the experimental results.

We chose $2CF_3$-UiO-66 for further stability evaluation. MOFs are commonly limited in practical applications due to their instability,[56–58] while UiO-66 is well known for its outstanding stability.[59,60] To test the stability of $2CF_3$-UiO-66, it was soaked in various solvents such as *N*,*N*-dimethylformamide (DMF), *N*,*N*-dimethylacetamide (DMA), toluene, *n*-hexane, dichloromethane (DCM), ethanol, methanol, and water for 24 h. The PXRD patterns showed no significant changes compared to that of the freshly prepared $2CF_3$-UiO-66 sample (Fig. S30–S32†). Furthermore, $2CF_3$-UiO-66 exhibited good stability under both acidic and basic aqueous conditions. After being soaked in aqueous solutions with various pH levels (ranging from 1 to 14) for 24 h, the PXRD patterns of $2CF_3$-UiO-66 remained unchanged (Fig. S33†). The thermal stability of $2CF_3$-UiO-66 was investigated by thermogravimetric analysis. $2CF_3$-UiO-66 started to decompose at 320 °C under an argon atmosphere (Fig. S34†). These stability evaluations of $2CF_3$-UiO-66 confirm its durability for applications in various environments.

To address the challenge that MOFs particles are difficult to recycle in practical separation applications, we next attempted to fabricate $2CF_3$-UiO-66 composite materials. We chose the fibrous cotton and porous sponge as MOFs carrier candidates. As illustrated in Fig. 2a, a piece of the cotton sheet (1.5 mm × 1.5 mm) was added to our MOFs synthesis reaction vessel with the $2CF_3$ ligands, $ZrCl_4$, and DMF. Upon heating at 100 °C for 24 h, we obtained the composite material, $2CF_3$-UiO-66@CT, with a $2CF_3$-UiO-66 mass loading of 27%. SEM images of the $2CF_3$-UiO-66@CT showed that $2CF_3$-UiO-66 nanoparticles were evenly distributed on the surface of cotton fibers with a diameter of ~200 nm (Fig. 2b and c). Elemental mapping results (Fig. 2d) are consistent with the SEM observations. PXRD patterns of $2CF_3$-UiO-66@CT showed characteristic peaks of UiO-66 at 7.34° and 8.52° and broad peak of cotton at 5°–10°, 14°–18° and 21°–25° (Fig. 2e), suggesting the successful incorporation of $2CF_3$-UiO-66 on cotton. Additionally, the hydroxyl groups on the surface of cotton fibers are proposed to coordinate with the metal sites of MOFs to enhance the stability of the composites.[61–63] FT-IR characterization (Fig. S44†) shows the peak intensity of the –OH band at 3430 cm^{-1} of $2CF_3$-UiO-66@CT is significantly decreased compared to that of cotton, which demonstrates the formation of coordination between the metal Zr and –OH groups.[64] The WCA of $2CF_3$-UiO-66@CT is 164.7° (Fig. 2f), qualifying a superhydrophobic material (WCA > 150°).[62] Moreover, water droplets roll smoothly on an inclined (30°) $2CF_3$-UiO-66@CT sample without leaving any traces (Fig. 2g). When $2CF_3$-UiO-66@CT contacts water in a beaker, it floats on the surface and cannot be wet (Fig. 2h). All these results indicate that $2CF_3$-UiO-66@CT is superhydrophobic.

$2CF_3$-UiO-66@CT was then tested for oil–water separation *via* filtration. We assembled an oil–water separation apparatus using $2CF_3$-UiO-66@CT and a syringe. $2CF_3$-UiO-66@CT was plugged at the bottom of a 5 mL syringe. Water (3 mL, containing 10 mM methylene blue indicator for visualization) was added to the syringe. Water was trapped above $2CF_3$-UiO-66@CT due to its superhydrophobic nature (Fig. S53a†). When water is pressed on the $2CF_3$-UiO-66@CT surface, its surface exhibits the mirror-like reflection characteristic of superhydrophobic materials (Fig. 3a). This phenomenon is due to a layer of air mixed between the superhydrophobic surface and the water interface. Subsequently, nine organic solvents (4 mL, containing 10 mM Sudan I indicator) were mixed with water (3 mL) and used to evaluate the oil–water separation efficiency. To demonstrate the versatility of oil–water separation *via* filtration using $2CF_3$-UiO-66@CT, we chose six representative solvents with a density smaller than water (gasoline, kerosene, hexadecane, *n*-hexane, petroleum ether, and toluene) and three with a density heavier than water (carbon tetrachloride, chloroform, and dichloromethane). The organic solvent and water mixture were poured into the filtration setup with a $2CF_3$-UiO-66@CT plug. All tested organic solvents passed through $2CF_3$-UiO-66@CT and were collected in a beaker while the water was retained in the syringe (Fig. 3b). Using this filtration method, the separation efficiency of these organic solvents and water is up to 99.66% (Fig. 3c). After separation by $2CF_3$-UiO-66@CT, the water content in gasoline and carbon tetrachloride was reduced to as low as 0.009% and 0.008%, respectively (Table 2, S8†). The isolated organic solvents from the water mixture using $2CF_3$-

Table 1 The liquid-water partition coefficients of different ligands

Ligands	BDC	1F-BDC	2F-BDC	$1CF_3$-BDC	$2CF_3$-BDC
$\log(P_{octanol}/P_{water})$	0.23	0.37	0.41	0.87	1.52

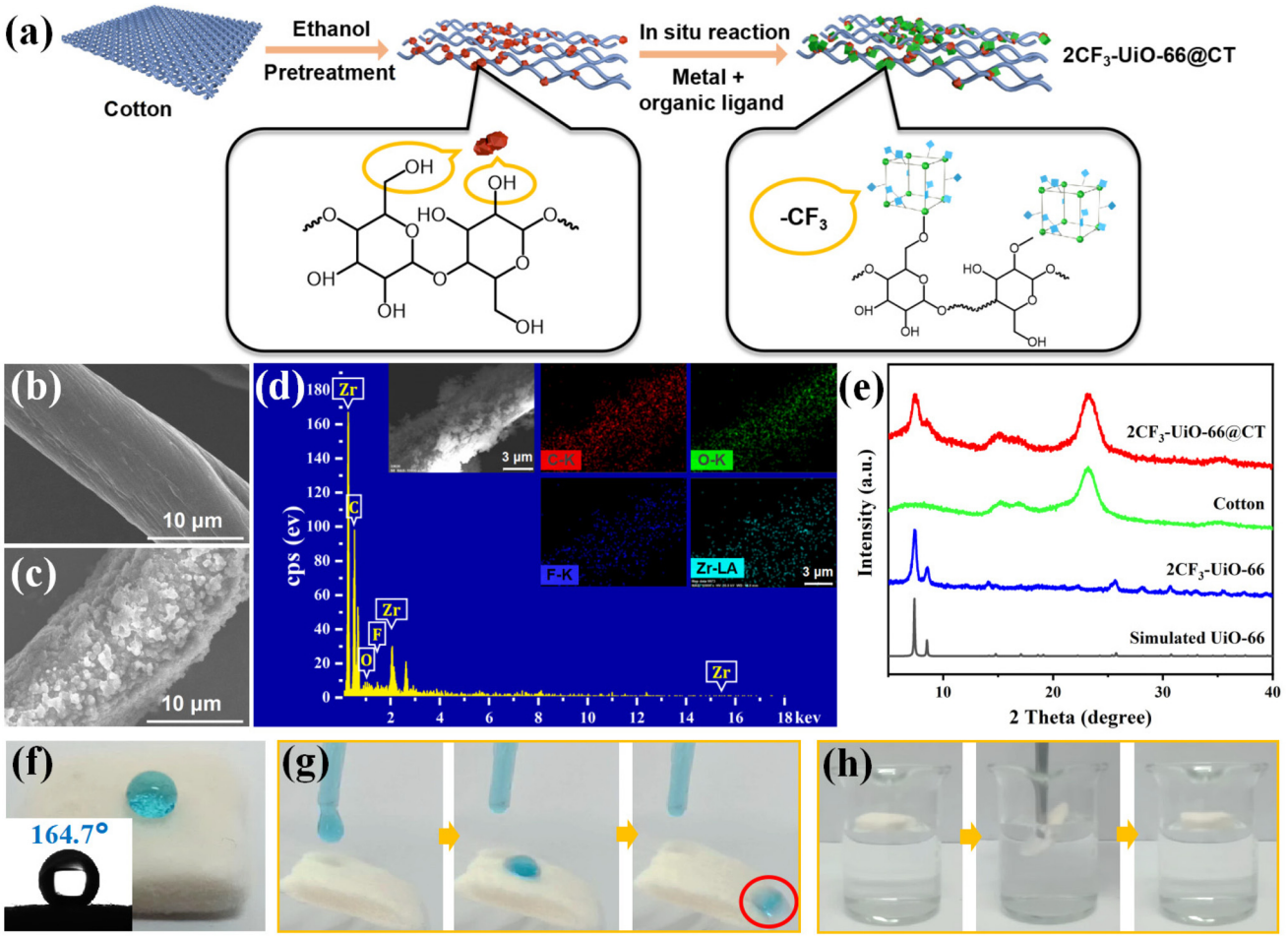

Fig. 2 (a) Schematic representation of the synthesis of $2CF_3$-UiO-66@CT. (b) SEM image of cotton fiber (c) SEM images of $2CF_3$-UiO-66@CT (d) SEM-EDX analysis of $2CF_3$-UiO-66@CT. (e) PXRD patterns of the simulated UiO-66, $2CF_3$-UiO-66, cotton and $2CF_3$-UiO-66@CT. (f) Image of a water (dyed with methylene blue) droplet on the surface of $2CF_3$-UiO-66@CT. The inset shows the contact angle. (g) Images of a water droplet (dyed with methylene blue) rolling on the inclined surface (30°) of $2CF_3$-UiO-66@CT. (h) Images of placing $2CF_3$-UiO-66@CT into deionized water.

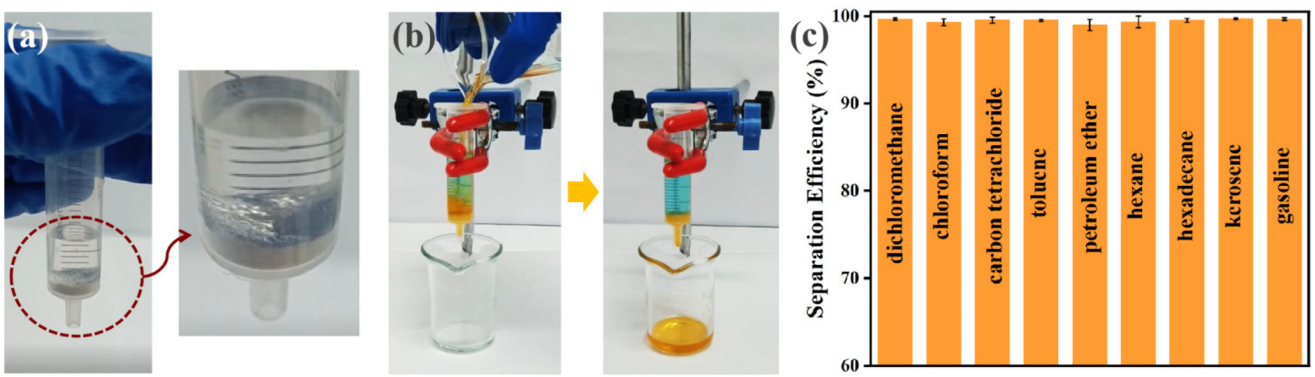

Fig. 3 (a) Images of $2CF_3$-UiO-66@CT separation device after adding 1 mL of deionized water (b) images of oil–water separation process using $2CF_3$-UiO-66@CT. Organic solvent (4 mL, containing 10 mM of Sudan I indicator for visualization) was mixed with deionized water (3 mL). The organic solvent could pass through $2CF_3$-UiO-66@CT while water was trapped. (c) The separation efficiency of different organic solvents and water using $2CF_3$-UiO-66@CT.

Table 2 The water content of gasoline after oil–water separation

No.	Sample	Water content (%)
1	No. 92 gasoline	**0.0096**
2	The mixed solution was separated once by $2CF_3$-UiO-66@CT material	0.0086
3	The mixed solution was separated ten times by $2CF_3$-UiO-66@CT material	0.0066

UiO-66@CT meet the commercial grade standard, highlighting its promising application in oil–water separation. Besides the separation efficiency, another possible concern in oil–water separation applications is the filtration rate. In a test run to separate dichloromethane from water (165 mm), the average filtration rate reached 10.87 cm^3 s^{-1} (Fig. S57†). The result indicates that $2CF_3$-UiO-66@CT has excellent permeability for organic solvents.

The flame retardancy of materials is also very important in the transportation and preservation of materials. We compared the flame retardancy of uncoated cotton and $2CF_3$-UiO-66@CT using a flame combustion method. The uncoated cotton is highly flammable and continued burning after the flame source was removed, leaving a black charred residual (Fig. 4a). Even if the backside of the cotton was not lit, it still changed color (Fig. 4d and e). In comparison, we attempted to ignite the $2CF_3$-UiO-66@CT with a lighter from the corner. Due to the surface coating of the flame-resistant $2CF_3$-UiO-66, $2CF_3$-UiO-66@CT did not catch on fire. Once the fire source was removed, the flame self-extinguished within 1 second (Fig. 4b). Only the part exposed to the flame turned black (Fig. 4f), and the majority of $2CF_3$-UiO-66@CT kept its original shape and color (Fig. 4g). To further test the flame retardancy of $2CF_3$-UiO-66@CT, we fully exposed one side to fire, but the backside remained unchanged (Fig. 4c and h–i), which proves the excellent flame retardancy of the $2CF_3$-UiO-66@CT composite. To quantify the flame retardancy of $2CF_3$-UiO-66@CT, we measured and compared its limiting oxygen index (LOI) with that of cotton. According to GB/T 5454-1997, the composite cotton material was prepared with a size of 58 mm × 150 mm. The LOI of uncoated cotton is 18.5%, while the LOI of $2CF_3$-UiO-66@CT is improved to 23.5% (Table S9†), indicating that $2CF_3$-UiO-66 and natural cotton fiber composite can effectively improve the flame-retardant ability of cotton. The oxygen content in the natural air is about 19%. In practical applications, composite cotton fiber can play its flame retardant fruit and effectively reduce economic losses. These results demonstrate the excellent flame retardant property of $2CF_3$-UiO-66@CT, which is beneficial for its practical storage, transpiration, and applications.

Using a similar one-pot synthetic method, $2CF_3$-UiO-66 and sponge composites ($2CF_3$-UiO-66@SP) were successfully prepared with a MOF mass loading of 24% (Fig. 5a). Similar to the size of $2CF_3$-UiO-66 particles on $2CF_3$-UiO-66@CT, SEM images of $2CF_3$-UiO-66@SP (Fig. 5b and c) revealed that $2CF_3$-UiO-66 particles with a diameter of 200 nm were uniformly coated on the surface of the sponge. Elemental mapping data and EDX confirmed the presence of $2CF_3$-UiO-66 on the sponge (Fig. S41†). PXRD patterns (Fig. 5d) exhibited sharp characteristic peaks at 7.34° and 8.52° from $2CF_3$-UiO-66 and broad peaks (5°–10° and 18°–25°) from the sponge. These characterizations indicated the successful synthesis of $2CF_3$-UiO-66@SP. $2CF_3$-UiO-66@SP is superhydrophobic with a WCA of 162.0° (Fig. S46b†). Compared with $2CF_3$-UiO-66@CT, $2CF_3$-UiO-66@SP has a porous sponge substrate, making it suitable for oil–water separation *via* adsorption. The adsorption capacity of $2CF_3$-UiO-66@SP for nine representative organic solvents (gasoline, kerosene, hexadecane, *n*-hexane,

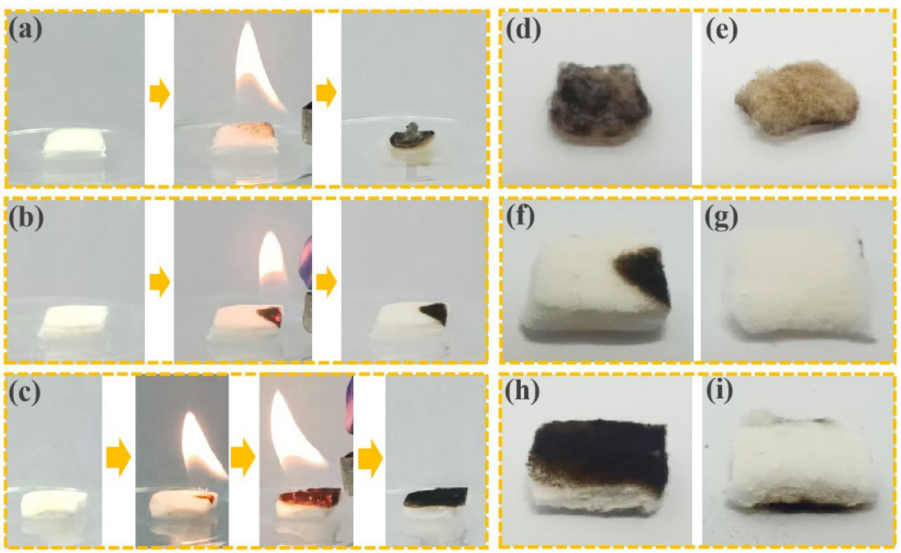

Fig. 4 Burning state of cotton kindling (a) and $2CF_3$-UiO-66@CT igniting part (b) and igniting whole side (c); the morphology of $2CF_3$-UiO-66@CT ignition surface and unignited surface of cotton (d and e) and combustion part (f and g) and combustion whole side (h and i).

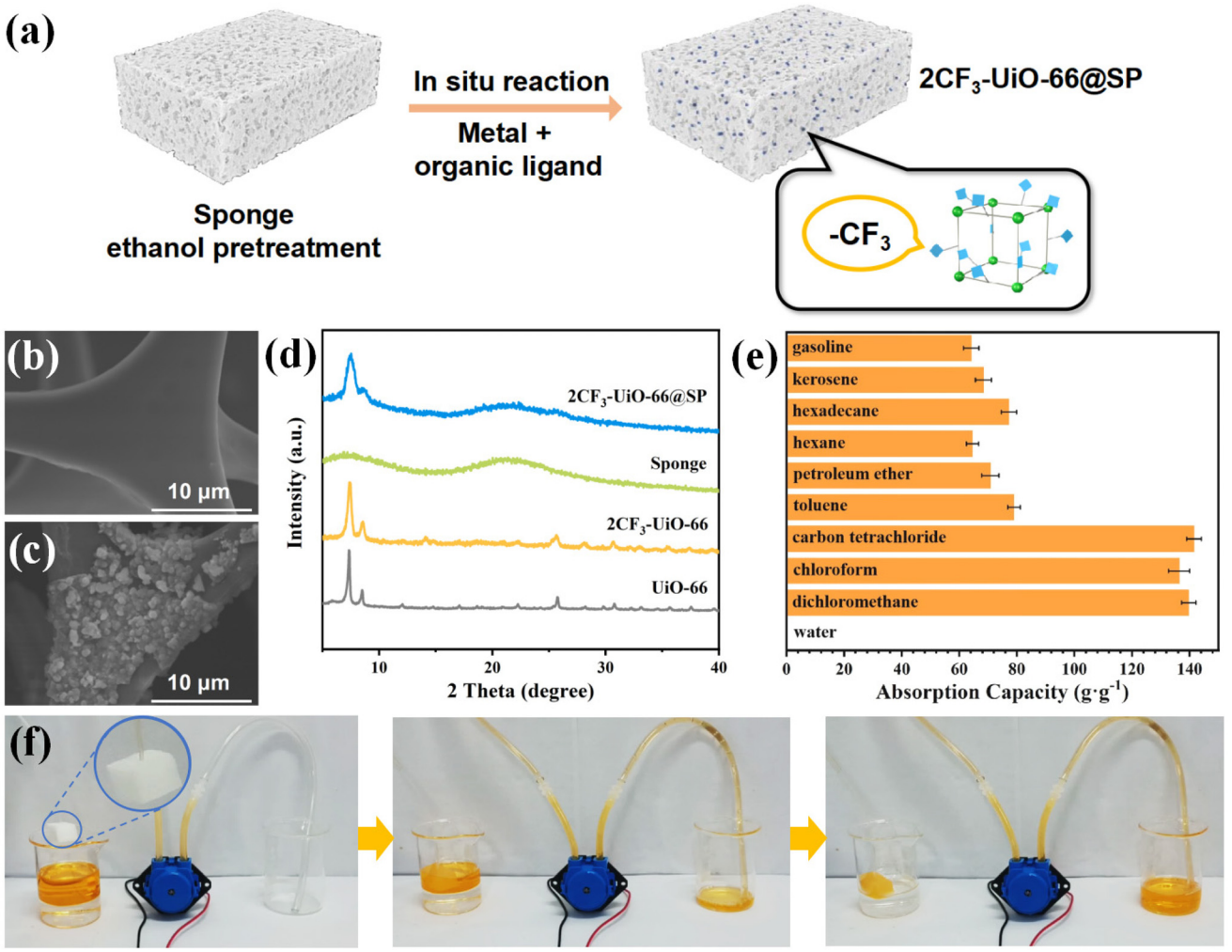

Fig. 5 (a) Schematic representation of the synthesis of $2CF_3$-UiO-66@SP (b) SEM image of sponge. (c) SEM image of $2CF_3$-UiO-66@SP. (d) PXRD experimental data of $2CF_3$-UiO-66@SP, sponge, $2CF_3$-UiO-66, and UiO-66. (e) The adsorption capacity of $2CF_3$-UiO-66@SP for different solvents. (f) Images of automatic light oil (dyed with Sudan I) adsorption device and its separation process using $2CF_3$-UiO-66@SP.

petroleum ether, toluene, carbon tetrachloride, chloroform, and dichloromethane) fell in the range from 64.15 to 141.52 g g^{-1} (Fig. 5e). It is comparable to the highest value reported in the literature (Table S13†). We proposed that such a high adsorption capacity is attributed to the synergistic effect of hydrophobic $2CF_3$-UiO-66 nanoparticles and the porous sponge. In sharp contrast, due to the superhydrophobic nature of $2CF_3$-UiO-66@SP, its adsorption capacity for water is only 0.15 g g^{-1}.

We aimed to apply $2CF_3$-UiO-66@SP in oil–water separation *via* anti-gravity adsorption (Fig. S58†). Carbon tetrachloride (1.5 mL) and water (6 mL) were added to a test tube. $2CF_3$-UiO-66@SP was added and pushed to the bottom. Immediately (within 2 seconds), we observed that the carbon tetrachloride was completely adsorbed upward by $2CF_3$-UiO-66@SP. Because of the superhydrophobicity of $2CF_3$-UiO-66@SP, carbon tetrachloride was separated from water and collected in a beaker. Inspired by the outstanding adsorption capacity of $2CF_3$-UiO-66@SP toward non-polar organic solvents, we designed another setup for automatic light oil adsorption and separation (Fig. 5f). $2CF_3$-UiO-66@SP was connected to a mechanical pump through a hose. To simulate the scenario of the light oil spill, light oil (10 mL) and water (10 mL) were mixed in a beaker. $2CF_3$-UiO-66@SP was then added, and it was suspended at the interface of water and light oil. $2CF_3$-UiO-66@SP rapidly adsorbed the light oil, and the adsorbed oil was pumped and collected in a clean beaker. The model setup demonstrated the great potential of $2CF_3$-UiO-66@SP in the separation of light oil and water, rendering $2CF_3$-UiO-66@SP as a promising material for oil–water separation *via* adsorption.

In addition, we evaluated the stability of composite materials. $2CF_3$-UiO-66@CT and $2CF_3$-UiO-66@SP were soaked in various solvents (kerosene, toluene, and carbon tetrachloride) and boiling water. The characteristic peaks of $2CF_3$-UiO-66 were still observed after the soaking test (Fig. S59 and S60†). We have also performed the mechanical stability of $2CF_3$-UiO-66@CT and $2CF_3$-UiO-66@SP characterizations,

including compression, stretching, and abrasion tests. After the mechanical treatment, there is no significant mass loss (Table S10†), and the PXRD patterns showed no significant changes compared to the original $2CF_3$-UiO-66 composites (Fig. S66†). In addition, the oil–water separation efficiency has not changed much either for both $2CF_3$-UiO-66@CT and $2CF_3$-UiO-66@SP (Fig. S67†). All these results indicate the high stability of $2CF_3$-UiO-66 composites. The durability of $2CF_3$-UiO-66@CT was also investigated. After repeating the filtration cycle twenty times with carbon tetrachloride, the PXRD patterns (Fig. S68†) showed no significant changes and the separation efficiency of $2CF_3$-UiO-66@CT has not significantly decreased (Fig. S69†).

4. Conclusions

In summary, we synthesized four fluorinated UiO-66 MOFs and demonstrated their potential applications in the adsorption of organic pollutants and oil–water separation. By comparing their water contact angle, vapor sorption, and the 3,5-dichlorophenol removal efficiency in water, we concluded that MOFs containing $-CF_3$ groups are significantly more hydrophobic than those containing –F. When the type of fluorine-containing functional group is the same, more fluorine substituents result in increased hydrophobicity. Additionally, an *in situ* synthetic method to prepare $2CF_3$-UiO-66@CT and $2CF_3$-UiO-66@SP composite materials was described. $2CF_3$-UiO-66@CT is superhydrophobicity and promising for oil–water separation *via* filtration with separation efficiencies exceeding 99%. Notably, the water content in the separated gasoline and carbon tetrachloride using $2CF_3$-UiO-66@CT was below 0.01%, meeting the standard of commercial reagents. Furthermore, $2CF_3$-UiO-66@CT exhibits good flame retardancy. Compared to $2CF_3$-UiO-66@CT, $2CF_3$-UiO-66@SP demonstrated excellent synergistic effects of the hydrophobic $2CF_3$-UiO-66 and porous sponge. $2CF_3$-UiO-66@SP with an adsorption capacity of 141.52 g g^{-1} for carbon tetrachloride. To the best of our knowledge, this is one of the highest values for similar materials regarding organic solvent adsorption capacity.[65] Combined with the conventional mechanical pump method for oil spill cleanup, $2CF_3$-UiO-66@SP showed promising results for the oil–water separation *via* anti-gravity adsorption. In addition, $2CF_3$-UiO-66@CT and $2CF_3$-UiO-66@SP show excellent solvent resistance and mechanical stability. We believe that fluorinated MOFs are promising materials for organic pollutant adsorption, superhydrophobic surface coating, and oil–water separation. They are potential solutions for marine oil spill cleanup. We also hope that our work will inspire the fabrication of novel MOF-based devices.

Author contributions

Y. Y. Jia conceived the project and provided funds. J. Q. Ma and L. Dong performed the experiments. J. Q. Ma and M. S. Zhang analyzed and interpreted the experimental data. R. Feng was responsible for DFT calculations. All the authors discussed the results and contributed to the preparation of the final manuscript.

Data availability

The data supporting this article have been included as part of the ESI.†

Conflicts of interest

The authors declare no conflict of interest.

Acknowledgements

This work is financially supported by National Natural Science Foundation of China (22361031), the Natural Science Foundation of Inner Mongolia Autonomous Region of China (2022QN02015), Research Program of Science and technology at Universities of Inner Mongolia Autonomous Region (NJZY22334).

References

1 M. Yang, B. Y. Zhang, X. J. Chen, Q. Kang, B. Y. Gao, K. Lee and B. Chen, Transport of microplastic and dispersed oil co-contaminants in the marine environment, *Environ. Sci. Technol.*, 2023, **57**, 5633–5645.
2 Z. Zhu, F. Merlin, M. Yang, K. Lee, B. Chen, B. Liu, Y. Cao, X. Song, X. Ye, Q. K. Li, C. W. Greer, M. C. Boufadel, L. Isaacman and B. Zhang, Recent advances in chemical and biological degradation of spilled oil: A review of dispersants application in the marine environment, *J. Hazard. Mater.*, 2022, **436**, 129260.
3 M. D. Hazaimeh and E. S. Ahmed, Bioremediation perspectives and progress in petroleum pollution in the marine environment: a review, *Environ. Sci. Pollut. Res. Int.*, 2021, **28**, 54238–54259.
4 R. M. Atlas and T. C. Hazen, Oil biodegradation and bioremediation: a tale of the two worst spills in U.S. history, *Environ. Sci. Technol.*, 2011, **45**, 6709–6715.
5 J. Beyer, H. C. Trannum, T. Bakke, P. V. Hodson and T. K. Collier, Environmental effects of the deepwater horizon oil spill: A review, *Mar. Pollut. Bull.*, 2016, **110**, 28–51.
6 A. L. Egan, B. L. Chilvers and S. Cassells, Does size matter? The direct economic costs associated with the MV Rena oil spill, *Mar. Pollut. Bull.*, 2021, **173**, 112978.
7 D. Kong, X. He, H. Yang and Z. Zhang, Experimental study for flame base drag and burning efficiency of spilled crude oil during *in situ* burning on water, *Process Saf. Environ. Prot.*, 2019, **131**, 48–54.

8 Z. Liu, J. Liu, Q. Zhu and W. Wu, The weathering of oil after the deepwater horizon oil spill: insights from the chemical composition of the oil from the sea surface, salt marshes and sediments, *Environ. Res. Lett.*, 2012, **7**, 035302.
9 B. Doshi, M. Sillanpaa and S. Kalliola, A review of bio-based materials for oil spill treatment, *Water Res.*, 2018, **135**, 262–277.
10 J. V. Mullin and M. A. Champ, Introduction/Overview to in situ burning of oil spills, *Spill Sci. Technol. Bull.*, 2003, **8**, 323–330.
11 H. Saini, E. Otyepková, A. Schneemann, R. Zbořil, M. Otyepka, R. A. Fischer and K. Jayaramulu, Hierarchical porous metal-organic framework materials for efficient oil-water separation, *J. Mater. Chem. A*, 2022, **10**, 2751–2785.
12 W. Hao, J. Xu, R. Li, X. Zhao, L. Qiu and W. Yang, Developing superhydrophobic rock wool for high-viscosity oil/water separation, *Chem. Eng. J.*, 2019, **368**, 837–846.
13 R. K. Gupta, G. J. Dunderdale, M. W. England and A. Hozumi, Oil/water separation techniques: a review of recent progresses and future directions, *J. Mater. Chem. A*, 2017, **5**, 16025–16058.
14 Y. Guan, F. Cheng and Z. Pan, Superwetting polymeric three dimensional (3D) porous materials for oil/water separation: A review, *Polymers*, 2019, **11**, 806.
15 S. A. Akbar Razavi and A. Morsali, Linker functionalized metal-organic frameworks, *Coord. Chem. Rev.*, 2019, **399**, 213023.
16 M. Woellner, S. Hausdorf, N. Klein, P. Mueller, M. W. Smith and S. Kaskel, Adsorption and detection of hazardous trace gases by metal-organic frameworks, *Adv. Mater.*, 2018, **30**, 1704679.
17 A. Fujiwara, J. Wang, S. Hiraide, A. Gotz, M. T. Miyahara, M. Hartmann, B. Apeleo Zubiri, E. Spiecker, N. Vogel and S. Watanabe, Fast gas-adsorption kinetics in supraparticle-based MOF packings with hierarchical porosity, *Adv. Mater.*, 2023, **35**, 2305980.
18 H. Lyu, O. I. F. Chen, N. Hanikel, M. I. Hossain, R. W. Flaig, X. Pei, A. Amin, M. D. Doherty, R. K. Impastato, T. G. Glover, D. R. Moore and O. M. Yaghi, Carbon dioxide capture chemistry of amino acid functionalized metal-organic frameworks in humid flue gas, *J. Am. Chem. Soc.*, 2022, **144**, 2387–2396.
19 X. Zhao, Y. Wang, D. S. Li, X. Bu and P. Feng, Metal-organic frameworks for separation, *Adv. Mater.*, 2018, **30**, 1705189.
20 R. B. Lin, S. Xiang, W. Zhou and B. Chen, Microporous metal-organic framework materials for gas separation, *Chem*, 2020, **6**, 337–363.
21 R. Rao, S. Ma, B. Gao, F. Bi, Y. Chen, Y. Yang, N. Liu, M. Wu and X. Zhang, Recent advances of metal-organic framework-based and derivative materials in the heterogeneous catalytic removal of volatile organic compounds, *J. Colloid Interface Sci.*, 2023, **636**, 55–72.
22 X. Wang, W. Zhou, S. Zhai, X. Chen, Z. Peng, Z. Liu, W. Q. Deng and H. Wu, Metal-organic frameworks: Direct synthesis by organic acid-etching and reconstruction disclosure as oxygen evolution electrocatalysts, *Angew. Chem., Int. Ed.*, 2024, **63**, 202400323.
23 Y. Zhou, R. Abazari, J. Chen, M. Tahir, A. Kumar, R. R. Ikreedeegh, E. Rani, H. Singh and A. M. Kirillov, Bimetallic metal-organic frameworks and MOF-derived composites: Recent progress on electro- and photoelectrocatalytic applications, *Coord. Chem. Rev.*, 2022, **451**, 214264.
24 Y. Wen, Á. Rentería-Gómez, G. S. Day, M. F. Smith, T. H. Yan, R. O. K. Ozdemir, O. Gutierrez, V. K. Sharma, X. Ma and H. C. Zhou, Integrated photocatalytic reduction and oxidation of perfluorooctanoic acid by metal-organic frameworks: Key insights into the degradation mechanisms, *J. Am. Chem. Soc.*, 2022, **144**, 11840–11850.
25 E. A. Dolgopolova, A. M. Rice, C. R. Martin and N. B. Shustova, Photochemistry and photophysics of MOFs: Steps towards MOF-based sensing enhancements, *Chem. Soc. Rev.*, 2018, **47**, 4710–4728.
26 Y. M. Jo, Y. K. Jo, J. H. Lee, H. W. Jang, I. S. Hwang and D. J. Yoo, MOF-based chemiresistive gas sensors: Toward new functionalities, *Adv. Mater.*, 2023, **35**, 2206842.
27 G. Xu, C. Zhu and G. Gao, Recent progress of advanced conductive metal-organic frameworks: Precise synthesis, electrochemical energy storage applications, and future challenges, *Small*, 2022, **18**, 2203140.
28 R. Zhao, Z. Liang, R. Zou and Q. Xu, Metal-organic frameworks for batteries, *Joule*, 2018, **2**, 2235–2259.
29 Y. Yang, Y. Guo, Z. Qiu, W. Gong, Y. Wang, Y. Xie and Z. Xiao, In situ growth of Zr-based metal-organic frameworks on cellulose sponges for Hg^{2+} and methylene blue removal, *Carbohydr. Polym.*, 2024, **328**, 121750.
30 S. Sağlam, F. N. Türk and H. Arslanoğlu, Use and applications of metal-organic frameworks (MOF) in dye adsorption: Review, *J. Environ. Chem. Eng.*, 2023, **11**, 110568.
31 Z. Wang, Y. Chen, L. Wang, J. Zheng, Y. Fan and S. Zhang, Rapid and efficient removal of toxic ions from water using Zr-based MOFs@PIM hierarchical porous nanofibre membranes, *Chem. Eng. J.*, 2023, **452**, 139198.
32 Y. Y. Jia, Y. H. Zhang, J. Xu, R. Feng, M. S. Zhang and X. H. Bu, A high-performance "sweeper" for toxic cationic herbicides: an anionic metal-organic framework with a tetrapodal cage, *Chem. Commun.*, 2015, **51**, 17439–17442.
33 B. Lalchawimawia, A. Sil, T. Banerjee, N. Singh, A. Bhatnagar, R. Mukhopadhyay and A. Mandal, Metal-organic framework-pesticide interactions in water: Present and future perspectives on monitoring, remediation and molecular simulation, *Coord. Chem. Rev.*, 2023, **490**, 215214.
34 K. Jayaramulu, F. Geyer, A. Schneemann, S. Kment, M. Otyepka, R. Zboril, D. Vollmer and R. A. Fischer, Hydrophobic metal-organic frameworks, *Adv. Mater.*, 2019, **31**, 1900820.
35 N. X. Zhu, Z. W. Wei, C. X. Chen, D. Wang, C. C. Cao, Q. F. Qiu, J. J. Jiang, H. P. Wang and C. Y. Su, Self-generation of surface roughness by low-surface-energy alkyl chains for highly stable superhydrophobic/superoleophilic

MOFs with multiple functionalities, *Angew. Chem., Int. Ed.*, 2019, **58**, 17033–17040.
36 Y. Liu, Z. Lin, Y. Luo, R. Wu, R. Fang, A. Umar, Z. Zhang, Z. Zhao, J. Yao and S. Zhao, Superhydrophobic MOF based materials and their applications for oil-water separation, *J. Cleaner Prod.*, 2023, **420**, 138347.
37 S. L. Yang, L. Peng, D. T. Sun, M. Asgari, E. Oveisi, O. Trukhina, S. Bulut, A. Jamali and W. L. Queen, A new post-synthetic polymerization strategy makes metal-organic frameworks more stable, *Chem. Sci.*, 2019, **10**, 4542–4549.
38 C. Yang, U. Kaipa, Q. Z. Mather, X. Wang, V. Nesterov, A. F. Venero and M. A. Omary, Fluorous metal-organic frameworks with superior adsorption and hydrophobic properties toward oil spill cleanup and hydrocarbon storage, *J. Am. Chem. Soc.*, 2011, **133**, 18094–18097.
39 Y. Chen, C. Peng, X. Liu, Z. Fu, B. Guo, W. Du, Y. Xu, B. Zeng, G. Chen, W. Luo, C. Yuan and L. Dai, Enter the multifunctional trifluoromethylated epoxy Resin: Excellent flame retardant, better dielectric, low thermal expansion, etc., *Chem. Eng. J.*, 2024, **481**, 148405.
40 J. Hou, L. Wang, X. Feng, J. Terada, L. Lu, S. Yamazaki, A. Su, Y. Kuwajima, Y. Chen, T. Hidaka, X. He, H. Wang and M. Ouyang, Thermal runaway of lithium-ion batteries employing flame-retardant fluorinated electrolytes, *Energy Environ. Mater.*, 2022, **6**, 12297.
41 T. Chen, C. Peng, C. Liu, C. Yuan, J. Hong, G. Chen, Y. Xu and L. Dai, Modification of epoxy resin with a phosphorus, nitrogen, and fluorine containing polymer to improve the flame retardant and hydrophobic properties, *Macromol. Mater. Eng.*, 2018, **304**, 1800498.
42 Y. T. Pan, Z. Zhang and R. Yang, The rise of MOFs and their derivatives for flame retardant polymeric materials: A critical review, *Composites, Part B*, 2020, **199**, 108265.
43 X. Qi, K. Liu and Z. Chang, Beyond powders: Monoliths on the basis of metal-organic frameworks (MOFs), *Chem. Eng. J.*, 2022, **441**, 135953.
44 M. Tsotsalas, H. Maheshwari, S. Schmitt, S. Heißler, W. Feng and P. A. Levkin, Freestanding MOF microsheets with defined size and geometry using superhydrophobic-superhydrophilic arrays, *Adv. Mater. Interfaces*, 2015, **3**, 1500392.
45 S. Zhang, X. Lu, X. Liu, K. Fang, J. Gong, J. Si, W. Gao and D. Liu, In situ generated UiO-66/cotton fabric easily recyclable for reactive dye adsorption, *Langmuir*, 2022, **38**, 12095–12102.
46 W. L. Li, K. X. Liu, Y. X. Zhang, S. Guo, Z. X. Li and S. C. Tan, A facile strategy to prepare robust self-healable superhydrophobic fabrics with self-cleaning, anti-icing, UV resistance, and antibacterial properties, *Chem. Eng. J.*, 2022, **446**, 137195.
47 W. L. Li, F. Q. Wang and Z. X. Li, A facile strategy for fabricating robust superhydrophobic and superoleophilic metal mesh via diazonium chemistry, *Colloids Surf., A*, 2021, **630**, 127570.
48 W. L. Li, Y. X. Zhang, S. Guo, Z. Yu, J. L. Kang, Z. X. Li, L. Wei and S. C. Tan, Multifunctional sandwich-structured super-hygroscopic zinc-based MOF-overlayed cooling wearables for special personal thermal management, *Small*, 2024, **20**, 2311272.
49 W. L. Li, X. T. Wang, Y. Wu, M. Q. Chen and Z. X. Li, One-step spontaneous grafting via diazonium chemistry for the fabrication of robust bionic multifunctional superhydrophobic fabric, *Surf. Coat. Technol.*, 2021, **407**, 126802.
50 Y. Chen, Q. Xiong, Y. Wang, Y. Du, Y. Wang, J. Yang, L. Li and J. Li, Boosting molecular recognition of acetylene in UiO-66 framework through pore environment functionalization, *Chem. Eng. Sci.*, 2021, **237**, 116572.
51 J. Zagorc-Koncan, A. Z. Gotvajn and T. Tisler, Hazard identification for 3,5-dichlorophenol in the aquatic environment, *Cell. Mol. Biol. Lett.*, 2002, **7**, 381–382.
52 H. Furukawa, F. Gándara, Y. B. Zhang, J. C. Jiang, W. L. Queen, M. R. Hudson and O. M. Yaghi, Water adsorption in porous metal-organic frameworks and related materials, *J. Am. Chem. Soc.*, 2014, **136**, 4369–4381.
53 S. I. Kim, T. U. Yoon, M. B. Kim, S. J. Lee, Y. K. Hwang, J. S. Chang, H. J. Kim, H. N. Lee, U. H. Lee and Y. S. Bae, Metal-organic frameworks with high working capacities and cyclic hydrothermal stabilities for fresh water production, *Chem. Eng. J.*, 2016, **286**, 467–475.
54 F. Neese, F. Wennmohs, U. Becker and C. Riplinger, The ORCA quantum chemistry program package, *J. Chem. Phys.*, 2020, **152**, 224108.
55 T. Lu and F. W. Chen, Multiwfn: A multifunctional wavefunction analyzer, *J. Comput. Chem.*, 2012, **33**, 580–592.
56 C. Wang, X. Liu, N. Keser Demir, J. P. Chen and K. Li, Applications of water stable metal-organic frameworks, *Chem. Soc. Rev.*, 2016, **45**, 5107–5134.
57 B. Pramanik, R. Sahoo and M. C. Das, pH-stable MOFs: Design principles and applications, *Coord. Chem. Rev.*, 2023, **493**, 215301.
58 M. Ding, X. Cai and H. L. Jiang, Improving MOF stability: approaches and applications, *Chem. Sci.*, 2019, **10**, 10209–10230.
59 J. H. Cavka, S. Jakobsen, U. Olsbye, N. Guillou, C. Lamberti, S. Bordiga and K. P. Lillerud, A new zirconium inorganic building brick forming metal organic frameworks with exceptional stability, *J. Am. Chem. Soc.*, 2008, **130**, 13850–13851.
60 C. G. Piscopo, A. Polyzoidis, M. Schwarzer and S. Loebbecke, Stability of UiO-66 under acidic treatment: Opportunities and limitations for post-synthetic modifications, *Microporous Mesoporous Mater.*, 2015, **208**, 30–35.
61 H. Singh Jhinjer, M. Jassal and A. K. Agrawal, Metal-organic frameworks functionalized cellulosic fabrics as multifunctional smart textiles, *Chem. Eng. J.*, 2023, **478**, 147253.
62 R. Dalapati, S. Nandi, C. Gogoi, A. Shome and S. Biswas, Metal-organic framework (MOF) derived recyclable, superhydrophobic composite of cotton fabrics for the facile removal of oil spills, *ACS Appl. Mater. Interfaces*, 2021, **13**, 8563–8573.

63 W. Li, Y. Zhang, Z. Yu, T. Zhu, J. Kang, K. Liu, Z. Li and S. C. Tan, In situ growth of a stable metal-organic framework (MOF) on flexible fabric via a layer-by-layer strategy for versatile applications, *ACS Nano*, 2022, **16**, 14779–14791.
64 T. I. Shaheen, S. S. Salem and S. Zaghloul, A new facile strategy for multifunctional textiles development through in situ deposition of SiO_2/TiO_2 nanosols hybrid, *Ind. Eng. Chem. Res.*, 2019, **58**, 20203–20212.
65 N. Habibi, S. Faraji and A. Pourjavadi, Nano graphite platelets/Cu (BDC) MOF coating on polyurethane sponge: A superhydrophobic self-extinguishing adsorbent for static and continuous oil/water separation, *Colloids Surf., A*, 2023, **676**, 132186.